MODELING QUANTITATIVE ACOUSTIC MICROSCOPY FOR LAYERED COATINGS

Zhiqi Guo and J. D. Achenbach
Center for Quality Engineering and Failure Prevention
Northwestern University
Evanston, IL 60208

INTRODUCTION

Multilayered ceramic and metallic coatings are receiving much attention for applications to improve the resistance to wear of surfaces. To assure the integrity of such coatings, quantitative nondestructive techniques are needed to determine the properties of coating materials and to evaluate the bonding quality of the interface between the coating and the substrate.

In this paper, the line-focus acoustic microscopy technique (LFAM) is applied to obtain quantitative information at high accuracy. In earlier work, this technique has been successfully applied to determine material constants of single-layer thin films, under the assumption that the interfacial conditions are perfect [1-2]. In this paper, we will go further, to extend the use of LFAM to multilayered thin films or coatings with perfect or imperfect interfacial conditions.

LFAM is a model-based technique. The final results for material constants are obtained by minimizing the difference between theoretical predictions and experimental measurements. Therefore a predictive model is essential. The main objective of the work reported here is to model quantitative line-focus acoustic microscopy for multilayered thin coatings or films with perfect or imperfect interfacial conditions, for applications, such as

- to determine the material constants of each layer in a layered coating,
- to quantitatively evaluate the bond between the layered coating and the substrate.

MEASUREMENT PRINCIPLE OF LFAM AND A V(z) MEASUREMENT MODEL

Figure 1a shows the cross-sectional configuration of the acoustic probe and a coated specimen. The acoustic probe consists of a buffer rod with a transducer at one end and a cylindrical lens at the other. An RF tone-burst excites the transducer to generate ultrasonic waves. The generated ultrasonic waves propagate through the buffer rod and are focused by the lens into a line-focused beam and coupled to the specimen through a coupling-fluid, usually distilled water.

Review of Progress in Quantitative Nondestructive Evaluation, Vol. 18
Edited by Thompson and Chimenti, Kluwer Academic/Plenum Publishers, 1999

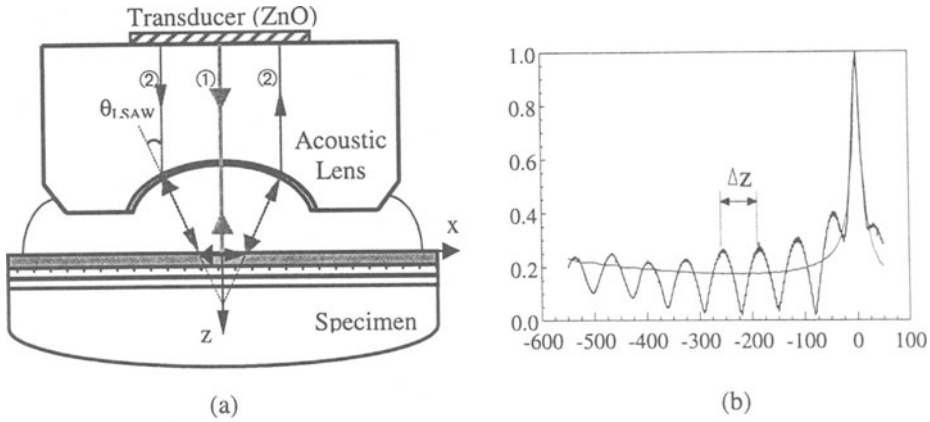

Figure 1. (a) Cross-sectional configuration of the acoustic probe and a coated specimen, (b) a typical V(z) curve.

After interacting with the specimen, the line-focused beam is reflected and returned to the transducer to produce a voltage output.

The technique used in this paper is based on the measurement of the so-called V(z) curve, which is a recording of the voltage output as a function of the distance between the lens and the specimen. Moving the acoustic probe toward the specimen changes the amount of defocus. Figure 1b shows a typical V(z) curve.

Two major components contribute to the V(z) curve. One is the directly reflected component, beam ①, the other is the typical leaky surface acoustic wave component, beam ②, which is excited by critical angle incidence. These two beams interfere with each other to cause the periodic dips in the corresponding V(z) curve when defocusing changes their phases.

The phase velocity of the leaky surface wave c can be determined from the interval, Δz, of the periodic dips, using equation (1).

$$c = c_w \cdot \left[1 - \left(1 - \frac{c_w}{2f \cdot \Delta z}\right)^2\right]^{-1/2} \approx \sqrt{c_w \cdot f \cdot \Delta z} \qquad (1)$$

where c_w is the wave velocity in water, and f is the operating frequency.

The interval Δz can be accurately extracted from the measured V(z) curve by spectrum analysis, as detailed in reference [3]. Therefore, through measuring V(z) curves on a specimen at different frequencies or different wave propagation directions, the experimental dispersion curves or directional variations of the leaky surface wave velocity can be obtained.

By numerically simulating the V(z) measurement procedure, theoretical V(z) curves are obtained and a V(z) measurement model can be developed to predict the phase velocity c for a layered specimen of arbitrary configuration.

In this paper, we use the approach proposed by Achenbach et al. [4] for synthesizing V(z) curves. In that approach, the output of the line-focus acoustic probe is expressed as a Fourier integral over the product of the characteristic functions of the acoustic lens, $L_1(k_x)$ and $L_2(k_x)$, and the reflectance function of a fluid-loaded specimen $R(k_x)$, as expressed in equation (2),

$$V(z) = \int_{-\infty}^{+\infty} L_1(k_x) \cdot L_2(k_x) \cdot R(k_x) \cdot \exp(2ik_z z) \cdot dk_x \qquad (2)$$

where (k_x, k_z) defines the wave vector, $k_z = \sqrt{k_w^2 - k_x^2}$, $k_w = \frac{c_w}{\omega}$, $k_x = \frac{c}{\omega}$.

The characteristic functions, $L_1(k_x)$ and $L_2(k_x)$, for the line-focus acoustic probe used for our laboratory have been analytically determined. We still need to derive the reflectance function for a general layered specimen with perfect or imperfect interfacial conditions.

REFLECTANCE FUNCTION FOR A LAYERED MEDIUM WITH PERFECT OR IMPERFECT INTERFACES

Figure 2 shows the schematic configuration of a layered medium. A time-harmonic plane wave is incident from a coupling fluid, at arbitrary incident angle θ. It follows from Snell's law that all the layers share certain field quantities, such as the frequency f and the velocity c.

The response of the layered medium to the incident waves can be expressed in terms of reflection and transmission coefficients. The reflection coefficient carries information on the layered medium, including the material properties and the thickness of each layer, and the interfacial conditions. A theoretical model can quantitatively relate these characteristic properties of the layered specimen to the corresponding reflectance function. Such a model has been developed by performing the following steps.

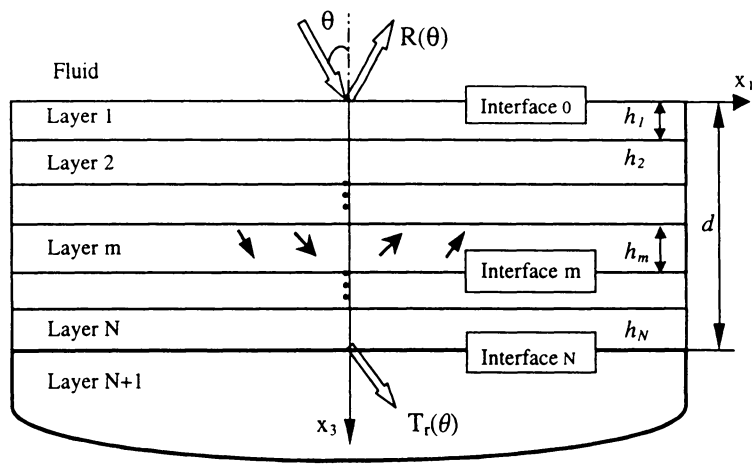

Figure 2. Schematic configuration of a multiple layered medium.

1. Find general wave field solutions for each layer to relate the state vector at an arbitrary location to the material properties, using the same method as used by Mal [5], and Chimenti and Nayfeh [6-7].
2. Model the interfacial zone by introducing characteristic parameters to represent the effects of the interface. Two models are considered for this purpose, namely, the spring model and a layer model.
3. Apply the transfer matrix method to construct a global transfer matrix to relate the state vector at the very top of the layered specimen to that at the very bottom.
4. Derive the expression for the reflectance function by enforcing the boundary conditions at the top and at the bottom of the layered specimen.

Because the thickness of the interfacial zone between the thin coating and the substrate is much smaller than the wavelength, the interface can be considered physically as a layer of springs. Three stiffness parameters (K_L, K_{T1}, K_{T2}) are needed to characterize the interfacial zone for anisotropic cases; for isotropic cases, only two stiffness parameters (K_L, K_T) are needed.

Equation (3) shows the relations between the stresses and the displacement discontinuities across the layer of springs. It can also be written in matrix form by defining the transfer matrix of the interface $[T_{int}]$.

$$\begin{Bmatrix} \sigma_{13} = K_{T1}\cdot(u_1^+ - u_1^-) \\ \sigma_{23} = K_{T2}\cdot(u_2^+ - u_2^-) \\ \sigma_{33} = K_L\cdot(u_3^+ - u_3^-) \end{Bmatrix} \qquad [T_{int}] = \begin{bmatrix} 1 & 0 & 0 & 0 & 0 & \frac{1}{K_{T1}} \\ 0 & 1 & 0 & 0 & \frac{1}{K_{T2}} & 0 \\ 0 & 0 & 1 & \frac{1}{K_L} & 0 & 0 \\ 0 & 0 & 0 & 1 & 0 & 0 \\ 0 & 0 & 0 & 0 & 1 & 0 \\ 0 & 0 & 0 & 0 & 0 & 1 \end{bmatrix} \tag{3}$$

The global transfer matrix [T] is the multiplication of transfer matrices of each layer and the interfacial zone as in equation (4). Delta-matrix reformulation (noted by *) is adopted to avoid the "precision problem" for the numerical calculations, which is implemented by using the Mathematica 3.0 software package.

$$[T] = [T_1]\cdot[T_2]\cdots[T_N]\cdot[T_{int}]\cdot[T_{N+1}] \text{ and } [T]^* = [T_1]^*\cdot[T_2]^*\cdots[T_N]^*\cdot[T_{int}]^*\cdot[T_{N+1}]^* \tag{4}$$

Equation (5) shows the expression for the reflectance function:

$$R = \frac{A - \beta\cdot B}{A + \beta\cdot B}, \quad \text{where} \quad \beta = \frac{ik_x\rho_f c^2}{\alpha_f} = \frac{i\rho_f\omega^2}{\alpha_f k_x}. \tag{5}$$

Here A and B are sub-matrices of the global transfer matrix [T] as detailed here for the anisotropic and isotropic cases, respectively.

$$A = \begin{vmatrix} T_{41} & T_{43} & T_{45} \\ T_{51} & T_{53} & T_{55} \\ T_{61} & T_{63} & T_{65} \end{vmatrix}, \qquad B = \begin{vmatrix} T_{31} & T_{33} & T_{35} \\ T_{51} & T_{53} & T_{55} \\ T_{61} & T_{63} & T_{65} \end{vmatrix} \qquad \text{for anisotropic cases,}$$

$$A = \begin{vmatrix} T_{31} & T_{33} \\ T_{41} & T_{43} \end{vmatrix} = T_{62}^{*}, \qquad B = \begin{vmatrix} T_{21} & T_{23} \\ T_{41} & T_{43} \end{vmatrix} = T_{52}^{*} \qquad \text{for isotropic cases.}$$

The reflection function can also serve for wave mode identification. The vanishing of its denominator, i.e., $|A+\beta \cdot B| = 0$, is exactly the characteristic equation of the layered specimen. Modal solutions can be obtained by numerically solving this equation. Setting $\beta = 0$ takes out the effects of the fluid loading, and thus the equation $|A| = 0$ can be used to identify the free wave modes. The reflection function itself can also be used to obtain modal solutions. It undergoes a -2π phase shift as the incident angle θ passes the critical angles θ_{crt}, which correspond to wave modes. Using this criterion to search the critical angles, the phase velocities of the wave modes can be calculated using the formula

$$c = \frac{c_w}{\sin \theta_{crt}}. \tag{6}$$

DATA INVERSION SCHEME

Figure 3 shows a general data inversion procedure. A numerical iterative searching algorithm, called the simplex method, is used to find a set of values that minimizes the deviation between the predicted and measured quantities. Equation (7) is the deviation function in terms of the measured and calculated quantities at N points, c_n and $\hat{c}_n$.

$$\text{Dev} = \frac{1}{N}\sum_{n=1}^{N}(c_n - \hat{c}_n)^2, \qquad \hat{c}_n = F(C_{ijkl}, K, d, f, \phi) \tag{7}$$

Here phase velocities are used, which are functions of material properties C_{ijkl}, interfacial parameters K, geometry d, and frequency f and wave propagation direction ϕ (for anisotropic materials). The phase velocities can be measured and calculated with respect to either frequency or wave propagation direction for different configurations.

APPLICATION OF THE MODEL AND THE DATA INVERSION SCHEME TO A THIN TWO-LAYER COATING

Figure 4 shows the configuration of a two-layer thin coating on a steel substrate. The thickness of each layer is measured separately and listed together with material properties in Table 1. Two stiffness parameters, i.e., the normal stiffness K_L and the tangential stiffness K_T, are introduced to characterize the interfacial zone.

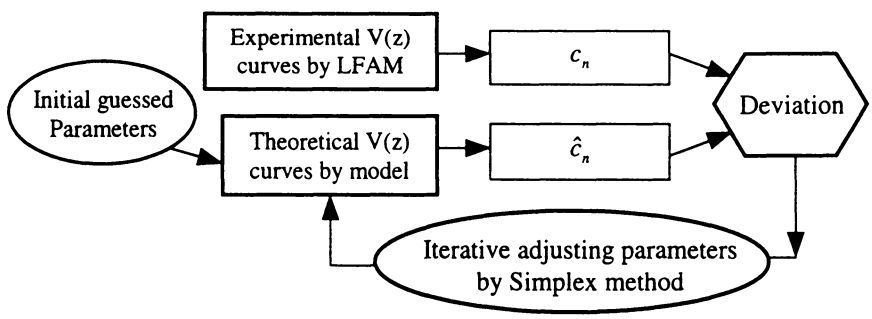

Figure 3. The general data inversion procedure.

Table 1. Material properties and thickness

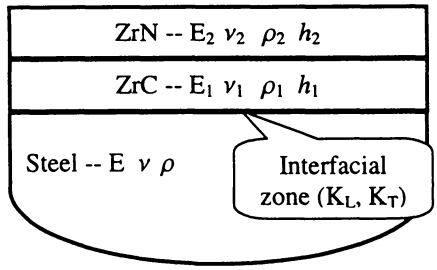

Material	ρ (g/cm^3)	h (μm)	E (GPa)	ν
Steel	7850		208.6	0.30
ZrC	5600	5.0	203	0.22
ZrN	7000	1.0	184	0.23

Figure 4. Configuration of a two-layer thin coating -- ZrC(5μm)/ZrN(1μm).

First consider perfect interfacial conditions. Four unknowns need to be determined, i.e., Young's modulus (E_1, E_2) and Possion's ratio (ν_1, ν_2) of each layer. The determined results are also listed in Table 1. A dispersion curve has been measured using LFAM at five different frequencies. The data inversion scheme is used to determine the four unknowns by fitting to the measured dispersion curve.

The theoretical dispersion curve calculated using the determined material constants is plotted together with the measured data in figure 5 to show the result of the data inversion method.

In order to investigate the uniqueness and accuracy of the data inversion, a convergence and sensitivity study was performed. The contour plots, figures 6a and 6b, show the deviation fields due to variations of the Young's moduli E_1 and E_2, and the Possion's ratios ν_1 and ν_2. Clearly, the convergence is good.

The cross-sectional variations of the deviation with respect to the material constants E_1, E_2 and ν_1, ν_2 can tell us how sensitive the deviation is to variations of those constants. The more sensitive the deviation, the more accurate the constants can be obtained. The results plotted in figures 6c and 6d show that the expected accuracy of E_1 is better than that of E_2, and better than that of both ν_1 and ν_2.

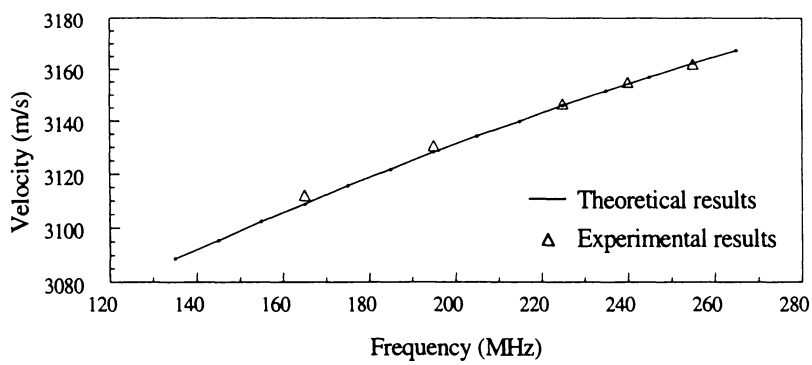

Figure 5. Measured and calculated dispersion curves.

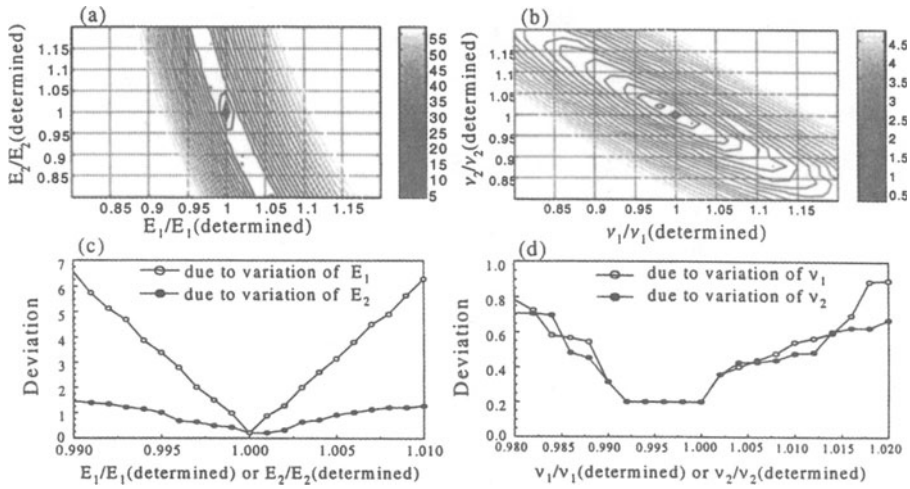

Figure 6. Deviation fields due to variations of E_1, E_2 in (a) and due to variations of ν_1, ν_2 in (b); Sensitivity of the deviation to material constants E_1, E_2 in (c) and ν_1, ν_2 in (d).

CHARACTERIZATION OF THE INTERFACIAL ZONE BETWEEN THE COATING AND SUBSTRATE

Through the model, the bond parameters K_l and K_t of the interfacial zone have been quantitatively related to the velocities of wave modes in the coating. Generally, this relation can be used to inversely determine the parameters. Figure 7 shows the calculated dispersion curves of the lowest wave mode in a two-layer coated specimen with various interfacial stiffness levels represented by the spring model. The results show that the dispersion relations are quite strongly affected by the interfacial conditions. From such curves, the stiffness parameters can be quantitative determined.

The characterization of the bond between a coating and a substrate involves additional unknowns whose uniqueness and accuracy need to be investigated. The goal is generally to determine all the unknowns from a single layered specimen by using sufficient data. The convergence and accuracy of data inversion for more than four unknowns are under investigation. Further research efforts will be required to determine the possible correlation between the introduced stiffness parameters and the strength of the bond.

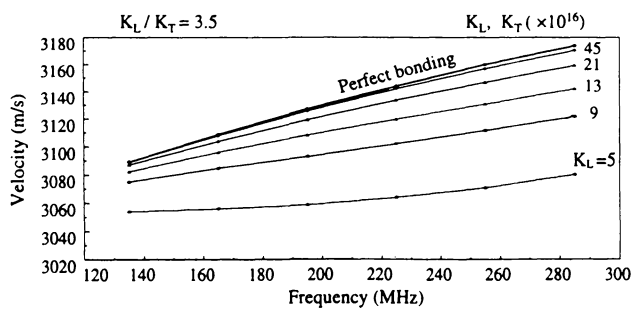

Figure 7. Calculated dispersion curves of the lowest wave mode in a two-layer ZrC/ZrN coating with various values of the bond parameters.

There are several possible applications of LFAM for characterization of the bond. The preparation of the surface of the substrate before coating deposition is very important for the bond quality. Which method is better can be determined through measuring the stiffness of the bond for a set of specimens that have been prepared by different methods. The degradation of a coating caused by fatigue or wear or by being exposed to a harsh environment may also be determined through measuring the change of the stiffness parameters of the bond.

CONCLUSIONS

A theoretical model for the reflectance function of multiple layered media has been developed. The layers can be isotropic or anisotropic with perfect or imperfect bond conditions. A convenient wave mode identification criterion was extracted from the derived reflectance function.

A V(z) measurement model has been developed to extend the LFAM to multiple layered thin films with imperfect interfaces.

A data inversion scheme was proposed and applied to determine the material constants of each layer in a two-layer thin coating.

The dispersion characteristic of a layered thin coating with various interfacial stiffness levels was calculated to show that LFAM has potential for characterization of the bond.

ACKNOWLEDGMENTS

This work was carried out in the course of research supported by the Office of Naval Research under Grant N00014-89-J-1362.

REFERENCES

1. J. Kushibiki, T. Ueda, and N. Chubachi, in *Proceedings of the 1987 IEEE Ultrasonic Symposium*, IEEE, Ed. New York, 1987, pp. 817-821.
2. J. O. Kim and J. D. Achenbach, Thin Solid Films, vol. 214, pp. 25-34, 1992.
3. J. Kushibiki and N. Chubachi, IEEE Trans. Sonics. Ultrason., vol. SU-32, pp. 189-212, 1985.
4. J. D. Achenbach, J. O. Kim, and Y.-C. Lee, in *Advances in Acoustic Microscopy*, vol. I, A. Briggs, Ed. New York: Plenum Press, 1995, pp. 153-208.
5. A. K. Mal, Int. J. Engng. Sci., vol. 26, pp. 873-881, 1988.
6. A. H. Nayfeh and D. E. Chimenti, Journal of Applied Mechanics, vol. 56, pp. 881-886, 1989.
7. A. H. Nayfeh, J. Acoust. Soc. Am., vol. 89, pp. 1521-1531, 1991.